

The resistivity phase diagram of cuprates revisited

D. Pelc^{1,*}, M. J. Veit^{1,‡}, M. K. Chan^{1,†}, C. J. Dorow^{1,§}, Y. Ge^{1,||}, N. Barišić^{1,2,3*} and M. Greven^{1,*}

¹ School of Physics and Astronomy, University of Minnesota, Minneapolis, MN 55455, USA

² Institute of Solid State Physics, TU Wien, 1040 Vienna, Austria

³ Department of Physics, Faculty of Science, University of Zagreb, HR–10000 Zagreb, Croatia

Present addresses:

[‡] Department of Applied Physics, Stanford University, Stanford, CA 94305, USA

[†] National High Magnetic Field Laboratory, Los Alamos National Laboratory, Los Alamos, NM 87545, USA

[§] Department of Physics, University of California, San Diego, CA 92093, USA

^{||} Department of Physics, Penn State University, University Park, PA 16802, USA

* correspondence to: dpelc@umn.edu, barisic@ifp.tuwien.ac.at, greven@umn.edu

The past three decades have seen extraordinary efforts to understand the cuprate high-transition temperature (high- T_c) superconductors. The phase diagram of these complex lamellar oxides is characterized by Mott-insulating and Fermi-liquid states at zero and high hole doping, respectively, and by an unusual regime at intermediate doping out of which the superconducting state emerges upon cooling. Here we report a detailed analysis of the temperature and doping dependence of the planar resistivity of simple tetragonal $\text{HgBa}_2\text{CuO}_{4+\delta}$ (Hg1201), the single- CuO_2 -layer cuprate with the highest optimal T_c . The data allow us to test a recently proposed phenomenological model that combines a universal scattering rate with spatially inhomogeneous (de)localization gap of the Mott-localized hole. We find that the model provides an excellent description of the data. We then extend this analysis to prior results for several other cuprates, and find little compound-to-compound variation in (de)localization gap scale. This points to a universal structural origin of the inherent gap inhomogeneity that is unrelated to doping-induced disorder.

At temperatures above T_c , the cuprates feature multiple electronic ordering tendencies, a partial depletion of states at the Fermi level (a ‘pseudogap’), and unusual transport (‘strange-metal’) behavior [1]. One of the most extensively investigated observables is the planar resistivity, ρ , which has long been known to exhibit several robust characteristics [2,3,4,5]: T -linear behavior above the doping-dependent pseudogap (PG) temperature, $T^*(p)$, which is most pronounced near optimal doping where T^* approaches T_c [3,4], and simple T^2 behavior at very high doping, where other measurements confirm Fermi-liquid (FL) behavior of itinerant quasiparticles [2,6,7]. Based on systematic resistivity data for a particular cuprate compound, the normal-state phase diagram can be obtained by evaluating the curvature (i.e., the second temperature derivative) of $\rho(T,p)$ [3]. Resistivity measurements thus provide indispensable information about the phase diagram of the cuprates, yet until recently, a comprehensive understanding of this pivotal observable had remained elusive.

In the theory of charge transport, the resistivity is generally parametrized with a charge-carrier density, effective mass, and scattering rate. In principle, all these quantities may be temperature- and doping-dependent, and therefore one needs additional insight to understand this observable. Two common assumptions made in evaluating the properties of the cuprates are that the resistivity is determined solely by the temperature dependence of the effective scattering rate and that the PG opens at doping-dependent temperature $T^*(p)$. The former assumption neglects the depletion of the density of states due to the opening of the PG, and hence the possibility that the carrier density depends on temperature, whereas the latter assumption overlooks the experimental evidence that local gaps already form at temperatures well above T^* [8]. In addition, several recent studies have shown that the itinerant carriers in the PG regime have FL character [5,9,10], and that an underlying FL-like transport scattering rate prevails through the entire phase diagram [11,12]. While these observations reveal a great degree of underlying simplicity, it is important to recognize that the cuprates are not ordinary Fermi liquids. In particular, photoemission results show an effectively disconnected Fermi surface (Fermi ‘arcs’) [13], NMR experiments [14] imply the existence of two local magnetic components – one associated with the PG and the other with the FL – and specific heat results are consistent with this scenario [15]. Moreover, numerous experiments, such as tunneling [8,16], magnetic resonance [17,18,19], X-ray [20] and neutron [21] scattering show that the cuprates are inhomogeneous, both structurally and electronically. However, a recent phenomenological model [22] rooted in three basic experimental facts – a temperature-dependent proliferation of PGs that commences at temperatures well above T^* , an underlying universal scattering rate for the itinerant carriers, and inhomogeneity – was found to successfully describe both the charge transport and the superfluid density of the cuprates. [22].

In the present work, our goal is three-fold: (i) to present a detailed resistivity phase diagram of the model cuprate Hg1201; (ii) to test if the data can be quantitatively described by the model of ref. [22], refining the analysis presented there; (iii) and to investigate how the model captures the similarities and subtle differences among cuprate families. Hg1201 is a remarkable cuprate [23]: it is structurally simple, with a tetragonal unit cell, and no known structural phase transitions; it can be hole-doped over a wide range using oxygen non-stoichiometry; and it features the highest optimal T_c of any single-layer cuprate. Furthermore, the effects of doping-induced point disorder

are similar to the ‘clean’ yet structurally more complex compound $\text{YBa}_2\text{Cu}_3\text{O}_{6+\delta}$ (YBCO) and relatively mild in comparison to, e.g., $\text{La}_{2-x}\text{Sr}_x\text{CuO}_4$ (LSCO) and the Bi-based cuprates. This is evidenced, e.g., by a nearly zero residual resistivity [5,11], the observation of quantum oscillations [24], the low level of superconducting vortex pinning [23,5], and the clear observation of a vortex lattice in small-angle neutron scattering measurements [25]. Finally, photoemission measurements indicate that the Fermi surface is simple near optimal doping [26], in contrast to, e.g., LSCO [27] and YBCO [28]. These properties render Hg1201 a model cuprate system, and its temperature-doping resistivity phase diagram should be representative of hole-doped cuprates. We find that this phase diagram can be comprehensively reproduced by the phenomenological model. Furthermore, we show that the model enables a quantitative description of the resistivity phase diagrams of other cuprate families by introducing small parameter variations. These findings highlight both underlying universal behavior and expected compound-specific features. Moreover, they point to a universal structural origin of the inherent gap inhomogeneity that is unrelated to doping-induced disorder.

Results

We analyze resistivity measurements on twelve Hg1201 single crystal samples, ranging from strongly underdoped to slightly overdoped (Fig. 1a). The dataset is that of ref. [11] with added new measurements for two samples (UD74 and OD90) and a slightly different estimate of sample sizes. Following previous work on other cuprate families [3], we plot the second temperature derivative of the resistivity, i.e., the resistivity curvature, in dependence on temperature and doping in Fig. 1b. The resulting phase diagram shows all the characteristic features present in other cuprates: two temperature scales in the underdoped region of the phase diagram, T^* and T^{**} , that correspond to a maximum in negative curvature and the onset of positive curvature, respectively; an extended region of approximately T -linear resistivity around optimal doping; and a slight positive curvature on the overdoped side of the phase diagram.

All these features can be quantitatively understood with a simple phenomenological model that we briefly describe in what follows (for details, see [22] and Methods). The three key ingredients of the model come from extensive experimental work. First, deep in the PG state, at temperatures below T^{**} ($T^{**} < T^*$), the itinerant carriers behave as a FL with carrier density p . The sheet resistance follows the simple scaling $\rho = A_{2s}T^2/p$ for a range of cuprates (that can be associated with the Drude expression for the resistivity) [5]; the magnetoresistance exhibits Kohler scaling for $T < T^{**}$ [9], a nontrivial characteristic of ordinary single-band metals; the optical scattering rate follows FL temperature/frequency scaling [10], and low-energy effective mass is approximately temperature- and doping-independent [10,29]. Finally, the temperature dependence of the transport scattering rate, as determined from the cotangent of the Hall angle (i.e., the inverse Hall mobility, μ^{-1}), is $\cot\Theta_H = \rho/\rho_{xy} = C_2T^2$ for $T < T^{**}$. In itself, this is not surprising, given the above observations and the fact that the Hall constant is approximately T -independent and a good measure of the doped carrier density ($R_H = 1/(ep)$, where e is the electron charge) for $T < T^{**}$ [11,30]. Remarkably, however, $\cot\Theta_H$ is quadratic in temperature and compound-independent (the coefficient C_2 is universal) throughout the PG and strange-metal regimes, and even upon approaching the well-established FL regime at high doping [11,12]. This

universal behaviour strongly suggests that the shape of the underlying Fermi surface does not change (in agreement with ARPES data [31]), but becomes pseudogapped, and that the scattering process is conventional electron-electron scattering that does not considerably change as the Mott insulator at zero doping is approached. This experimental fact of a nearly universal scattering rate is a crucial starting point of the model, which assumes that the mobility is always given by $1/\mu = C_2 T^2$, where T is the temperature and C_2 a material- and doping-independent constant (obtained from experiment). The second key ingredient of the model is a PG-induced change of the itinerant carrier concentration, with both temperature and doping. Here the main challenge is to connect the underdoped regime, where the low-temperature carrier concentration equals the nominal hole doping concentration p , to the overdoped regime, which is known to have a large Fermi surface with $1 + p$ carriers per unit cell. To make this connection, the model assumes the following. Each planar CuO_2 unit contains $1 + p$ holes, but p holes are always mobile, while 1 hole is separated from the Fermi level by a (doping-dependent) gap Δ . Essentially, this real-space gap corresponds to the k -space PG of the underlying large Fermi surface. The third and final ingredient is that the gap is taken to be inhomogeneous in real space, i.e., to vary from one CuO_2 unit to the next. This is quantified through a gap distribution function, and the effective density of itinerant carriers p_{eff} is obtained in a straightforward manner as the sum of the density p of doped carriers and a temperature- and doping-dependent density of delocalized carriers. The resistivity then is simply calculated using the standard Drude expression with the universal scattering rate and temperature- and doping-dependent effective carrier density. The only parameters to be specified are the gap distribution parameters: its width, skew, and doping dependence.

Figure 1c demonstrates that the model captures the normal-state phase diagram of Hg1201 with remarkable precision up to the highest measured temperature of 400 K. On the underdoped side, the gap distribution is far from the Fermi level, so that the low-temperature p_{eff} is just p and the resistivity is quadratic in temperature. The roughly T -linear resistivity regime appears when the gap distribution is close to the Fermi level, and holes can be continuously excited across the local gaps with increasing temperature. Beyond optimal doping, all the local gaps eventually close, and the full $1 + p$ Fermi surface is established. Yet this does not occur abruptly, due to the local gap inhomogeneity, but in a continuous manner [11,22]. Importantly, the results do not critically depend on the shape of the distribution: the phase diagrams and representative calculated resistivities are shown for three different skew parameters in Fig. 2. A strong skew pushes the linear- T regime down to lower temperatures, but the resistivity is always quadratic in the $T \rightarrow 0$ limit. We will return to this point below.

For an additional quantitative comparison between the model and experiment, we extract the low-temperature quadratic resistivity coefficient A_2 in the regime where $\rho = A_2 T^2$ ($T < T^{**}$, red in Fig. 1b,c), and the linear coefficient A_1 for $T > T^*$, similar to previous work [5]. As shown in Fig. 3, the model captures the data well. The doping dependence of A_2 is consistent with $A_2 \sim 1/p$ up to at least $p \sim 0.13$, whereas A_1 decreases somewhat more strongly with doping. Note also that model correctly captures the relative magnitudes of A_1 and A_2 . Importantly, in the doping range of the present study, there is no evidence for a doping-dependent effective mass, and hence the

linear coefficient here is inconsistent with the recent assertion of a universal ‘Planckian’ dissipation limit in cuprates [32].

Having demonstrated the success of this simple phenomenological model in Hg1201, we turn to resistivity phase diagrams for other cuprate families from Ref. [3]. Figure 4 shows a comparison for $\text{Bi}_2\text{Sr}_{2-z}\text{La}_z\text{CuO}_{6+x}$ (BSLCO) and YBCO. A comparison for LSCO was performed in previous work [22]. The gap distribution parameters for the four cuprate families are summarized in Table 1. Notably, other cuprates exhibit structural complications that are absent in Hg1201, including orthorhombic distortions (LSCO), superstructure (bismuth-based cuprates and Cu-O chains (YBCO)). Nevertheless, measurements of linear and quadratic resistivity coefficients show a nearly universal evolution with doping [5]. It is thus not surprising that the model is in good agreement with the respective experimental phase diagrams, employing quite similar gap distribution parameters. Clearly, the model with a skewed Gaussian gap distribution has enough flexibility to account for material-specific differences, while successfully capturing the universal features of the phase diagram. The gap distribution parameters for the different families are similar, with a somewhat smaller distribution width for YBCO. This points to a universal underlying mechanism of gap inhomogeneity in cuprates, which appears to be inherent to these lamellar perovskite-related oxides and at best weakly related to doping-induced disorder.

Discussion

The phenomenological model of ref. [22] provides a simple explanation of perhaps the most unusual feature of cuprate resistivity, the approximately linear- T behavior near optimal doping from low to high temperatures. This is achieved by forgoing the common assumption that the resistivity temperature dependence is solely determined by the scattering rate, an assumption that is especially far-reaching in the T -linear region, since a T -linear scattering rate is often interpreted as indicative of quantum critical fluctuations [33,34,35]. Yet this is clearly incompatible with the experimentally determined underlying universal scattering rate [11,12]. If the scattering rate is simple and quadratic in temperature and the effective mass virtually constant, as supported by experiment [10,29], Occam’s razor suggests that the nontrivial behavior of the resistivity is due to a temperature-dependent carrier density, as indeed supported by the modeling. Notably, this argument has been used in previous work to model the transport coefficients of underdoped cuprates [36,37] and is in agreement with Hall-effect measurements [30,38,39]. However, we stress that the underlying scattering rate remains quadratic, and in the limit of zero temperature the resistivity is quadratic as well. This is in contrast to the quantum critical point scenario [33,34,35], where the linear- T resistivity originates in scattering on quantum fluctuations near a critical point. In such a picture, the zero-temperature limit of the resistivity is linear, with possible deviations at higher temperatures [33]. In the cuprates it is notoriously difficult to determine the true low-temperature normal-state behavior, because of the extremely high magnetic fields needed to completely suppress superconductivity and the possibility of a field-induced modification of the normal state [4,40]. For compounds with lower critical fields, such as Nd-doped LSCO, there have been reports of low-temperature linear- T resistivity and Hall mobility [34]; yet we emphasize that these compounds are structurally and electronically complex, with several low-temperature structural transitions [41], incipient

structural instabilities [42] and high residual resistivities [3,34]. Furthermore, several cuprates (including La-based materials) feature a van Hove singularity in the density of states above optimal doping that should affect the low-temperature transport properties [43]. However, importantly, our focus is on the gross features of the phase diagram up to the comparatively high temperature/energy scale relevant for understanding the high- T_c phenomenon, and that can be understood without invoking quantum criticality. We note also that for YBCO [3] and Hg1201 (Fig. 1a) the low-temperature resistivity cannot be linear in temperature (with the same slope as at high temperature) around optimal doping. Namely, if one extrapolates the linear dependence above T_c to $T = 0$, one finds a *negative* residual resistivity, which is unphysical and implies that the resistivity must have curvature below T_c (in the hypothetical absence of superconductivity). Therefore, the linear- T resistivity above T_c is not representative of the underlying zero-temperature normal-state behaviour. Notably, both YBCO and Hg1201 have small residual resistivities [3,5] due to the relatively gentle effects of oxygen doping [44], but the same argument cannot be made for LSCO or BSLCO where point disorder (due to substitutional doping) induces large residual resistivities [3,4] and resistivity upturns [3,11,45].

Another important point is the absolute value of the resistivity, which can be fairly high compared to ‘good’ metals. Although it is often argued that the cuprates exceed the semiclassical Mott-Ioffe-Regel limit for coherent charge transport, arguments have been put forward that this assertion is in fact not correct [5,46]. The high resistivity values are mainly the result of a low density of charge carriers (with an underlying large Fermi surface), while the room-temperature Hall mobility of the cuprates such as Hg1201 is comparable to that of ordinary metals such as Aluminum [11]. We note also that there is in fact experimental evidence for an approach to resistivity saturation, e.g., in strongly underdoped LSCO at high temperatures [2,46]. Naturally, at high enough temperatures, the premises of our model will break down, in at least two possible ways: (i) additional scattering mechanisms such as optic phonons will modify the simple T^2 scattering rate; (ii) the resistivity values will approach saturation, yet at a significantly higher level than the semiclassical Mott-Ioffe-Regel limit [46]. However, since the available Hall mobility data up to 400 K show no evidence for these deviations, there is no need to include them in the modeling.

The resistivity phase diagram is rather insensitive to the different electronic ordering phenomena in underdoped cuprates, most importantly the formation of weak charge density wave (CDW) order [1]. Quasi-static two-dimensional CDW correlations with short coherence lengths and small amplitudes have been mapped as a function of doping and temperature in, e.g., in YBCO [47,48] and Hg1201 [49,50,51] via resonant X-ray scattering and found to be strongest in the underdoped part of the phase diagram, around $p \sim 0.1$ -0.12. In addition, dynamic CDW correlations are present in a wide doping/temperature range [52]. Yet no particular features related to the characteristic CDW temperatures are seen in the resistivity phase diagrams, and only slight downturns are visible in the (low field) Hall constant around $p \sim 0.1$ [11]. This strongly indicates that the CDW-induced Fermi surface reconstruction [49,53,54] is a secondary phenomenon that only occurs in high magnetic fields.

Notably, the mean gap scale Δ_m is also seen in photoemission and tunneling experiments [22,55], and it manifests itself as a broad peak in the optical conductivity, detected in several representative cuprate families [56,57]. It is the highest intrinsic gap scale in a hierarchy of (pseudo)gaps observed by different experimental probes in underdoped cuprates [22,55]. While firmly rooted in experiment, the model tested here is phenomenological and does not give microscopic insight into the origin of the local gap, its doping dependence, or the gap distribution function. It is based on the simplest possible assumptions on the mean gap and distribution width doping dependences, which may in reality be somewhat different, especially for strongly underdoped compounds close to the insulating phase [22,30]. Yet for Hg1201 and BSLCO, this is not much of a concern, since the accessible doping ranges are somewhat limited. The inhomogeneous gap can be interpreted as a localization gap, induced by strong electronic correlations. Accordingly, the extrapolated mean gap at zero doping is within a factor of two of the transport charge transfer gap [30]; this discrepancy can be remedied if a nonlinear gap dependence on doping is used [22]. The decrease of the localization gap with doping must be due to screening, and the model could thus be refined by obtaining the doping dependence of the gap distribution in a self-consistent way.

The good agreement with the experimental resistivity phase diagrams, using a doping-independent gap distribution width, is consistent with the finding of universal gap disorder in STM experiments [16]. Together with the weak compound dependence of the model parameters, this indicates that the inhomogeneity has an inherently structural origin. Namely, materials with perovskite or perovskite-derived structure are known to be prone to both long- and short-range structural instabilities and texturing [58,59,60]. Through a coupling of localized holes to the lattice, subtle structural disorder such as bond angle inhomogeneity can induce a localization gap distribution. This conclusion is supported by the observations that the tetragonal-to-orthorhombic structural transition in LSCO [61] corresponds to $\sim 100\%$ localization of one hole per unit cell [22], and that a subtle breaking of inversion symmetry has been observed in YBCO in a similar temperature/doping range [62].

To conclude, we have presented a comprehensive resistivity curvature phase diagram for the simple tetragonal cuprate Hg1201 and used this to test a recent phenomenological model for the normal state in a quantitative fashion. The model employs a renormalized gap scale that is linked to the charge-transfer gap of the undoped insulating state, and that constitutes the largest pseudogap scale at non-zero doping. We have demonstrated that the model is remarkably successful in reproducing the phase diagrams of other cuprate families as well, with nearly universal parameters. This universality implies that the considerable gap distribution is an inherent characteristic of the CuO_2 planes, and quite insensitive to the details of the crystal structure or doping method. However, the differences in model parameters for the different cuprate families (in particular the distribution widths) could provide important clues to the precise origin of the inhomogeneity, when combined with experiments that probe the local electronic structure.

Methods

Samples. The Hg1201 samples used in this work were grown and characterized according to established procedures [23,63]. Briefly, the single crystals are grown using an encapsulation method, and annealed in vacuum or oxygen to obtain the desired hole doping level. The doping level is determined from the value of T_c as obtained in Meissner effect measurements, as in previous work [64].

The model. The basic quantity to be calculated within the model is the effective carrier density. Taking into account the inhomogeneous localization gap, a gap distribution function $G(\Delta)$ is introduced, and the density of mobile carriers at a given temperature and doping generally becomes

$$p_{eff}(p, T) = p + \int_{-\infty}^{\infty} G(\Delta) e^{-\Delta/2kT} d\Delta \quad (1)$$

where k is Boltzmann's constant and T the temperature. The localized states are below the Fermi level, so we use Δ for the absolute value of the gap (to avoid the sign inconsistency between the equations and Fig. 1 in ref. [22]). To calculate p_{eff} (and all transport coefficients) the distribution function and its dependence on doping need to be specified. The simplest possible assumption is that each of the local gaps Δ decreases linearly with doping and closes eventually. At that point, the hole is no longer localized, and joins the Fermi sea at $T = 0$. The function $G(\Delta)$ will thus contain two parts: a contribution for positive Δ , and a delta-function contribution with a weight equal to the number of unit cells where $\Delta = 0$ at a given doping level. To parametrize the gap distribution, we use a skewed Gaussian of the form $g(\Delta) = 2\Phi(\alpha\tilde{\Delta})\varphi(\tilde{\Delta})$, where φ is a normalized Gaussian distribution, Φ its cumulative (i.e., the error function), α the skew parameter, and $\tilde{\Delta} = (\Delta - \Delta_m)/\delta$, with Δ_m the Gaussian mean gap and δ the Gaussian width. This parametrization allows a systematic investigation of the influence of distribution width and shape, yet it is purely phenomenological. Using the function g , the gap distribution in (1) becomes

$$G(\Delta) = g(\Delta)\theta(\Delta) + \delta(\Delta) \int_{-\infty}^0 g(\Delta') d\Delta' \quad (2)$$

where $\theta(\Delta)$ is the Heaviside (step) function and $\delta(\Delta)$ the Dirac delta function. The first term represents the unit cells with gapped holes, while the second term includes those unit cells whose gaps have closed, contributing to the Fermi sea at all temperatures. Furthermore, as noted above, we assume that the mean gap depends linearly on doping, as $\Delta_m = \Delta_0(1 - p/p_c)$, with Δ_0 the extrapolated mean gap at zero doping, and p_c the critical doping where the mean gap is zero. As the simplest possibility, we also take the width δ to be doping-independent. Therefore, four parameters uniquely determine the gap distribution and its doping dependence: Δ_0 , p_c , δ and the skew parameter α . Within the FL picture, the (dimensionless) resistivity is simply

$$\rho(p, T) = \frac{C_2}{p_{eff}(p, T)} T^2 \quad (3)$$

To obtain resistivity values, we use $C_2 = 0.0175 \text{ K}^{-2}$ from experiment [11,12] and multiply with the dimensional constant H/e (with H the magnetic field used for the C_2 measurements, in this

case 9 T). Notably, the value of C_2 is consistent with conventional electron-electron scattering estimates for the large underlying Fermi surface that encloses $1 + p$ carriers [65,66]. This Fermi surface is partially smeared out by the spatially inhomogeneous gaps, but can indeed be observed in photoemission experiments that integrate over a fairly broad energy range [31].

Acknowledgments.

The work at the University of Minnesota was funded by the Department of Energy through the University of Minnesota Center for Quantum Materials under DE-SC-0016371. The work at the TU Wien was supported by FWF project P27980-N36 and the European Research Council (ERC Consolidator Grant No 725521).

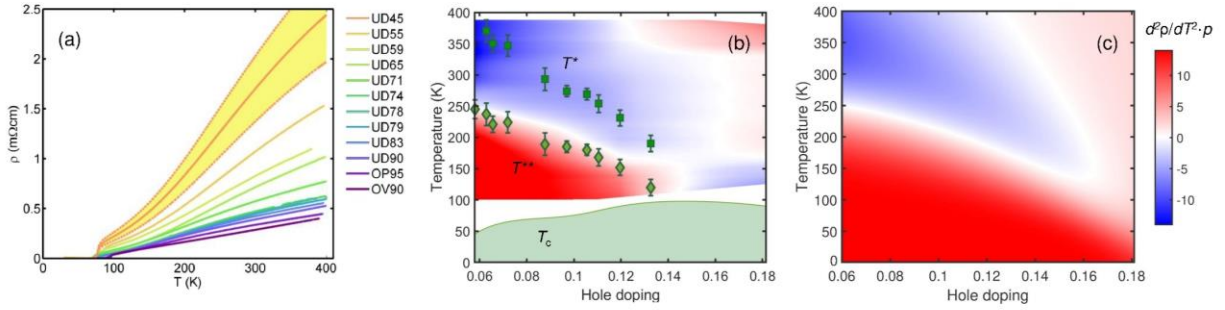


Figure 1 | Resistivity phase diagram of Hg1201. (a) Raw resistivity data for 12 single crystal samples of Hg1201, marked by their T_c values; UD, OP and OD represent underdoped, optimally doped, and overdoped samples, respectively. The band around the UD45 curve indicates the typical (relative) range of absolute value uncertainty due to crystal dimensions and contact distance (systematic error). Data for UD45 – UD71 and UD78 – OP95 are from ref. [11], and the data for UD74 and OD90 are new. (b) experimental and (c) calculated contour plot of the second temperature derivative (curvature) of the resistivity. The experimental plot is obtained from data in (a). The resistivity curvature is normalized by the hole doping p , which is obtained from T_c values, and the color scale is the same for (b) and (c). The symbols in (b) are the characteristic temperatures T^* and T^{**} obtained from experimental data: T^* is the temperature where the resistivity curves depart from high-temperature linear behavior, and at T^{**} they depart from the low-temperature quadratic behavior.

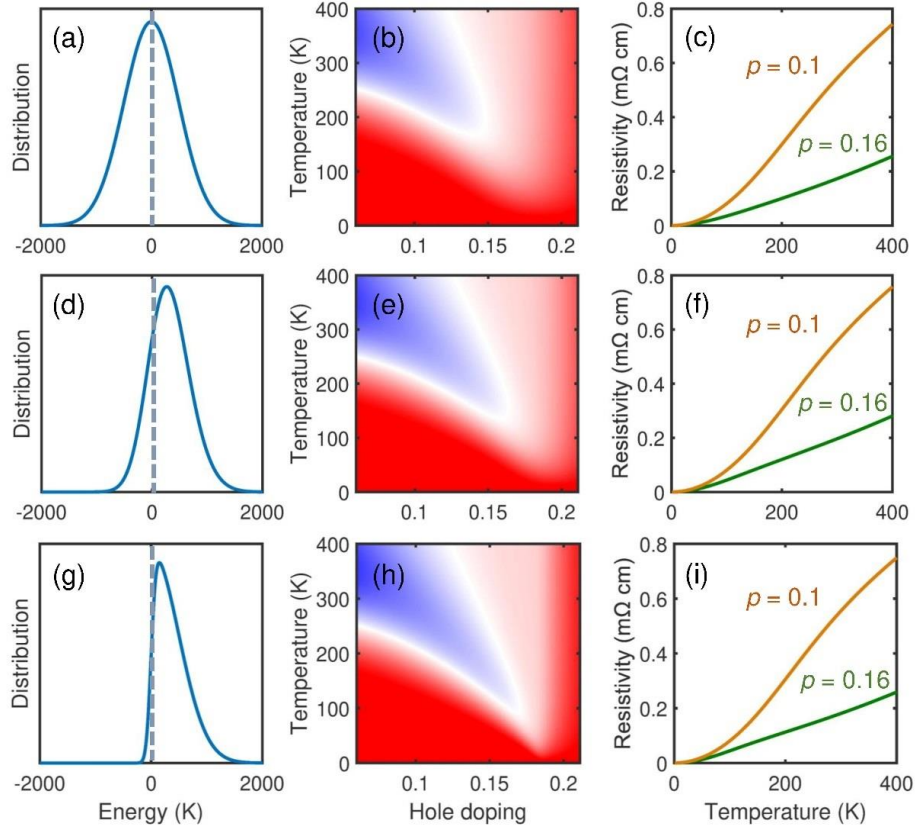


Figure 2 | Modeling of cuprate resistivity. Gap distribution functions, resistivity curvature phase diagrams and representative resistivity curves for three different values of the distribution skew parameter: (a)-(c), $\alpha = 0$ (pure Gaussian distribution); (d)-(f), $\alpha = 2$ (typically used for comparison with experiment); (g)-(i), $\alpha = 10$ (strong skew). The distributions are shown for $p = p_c$.

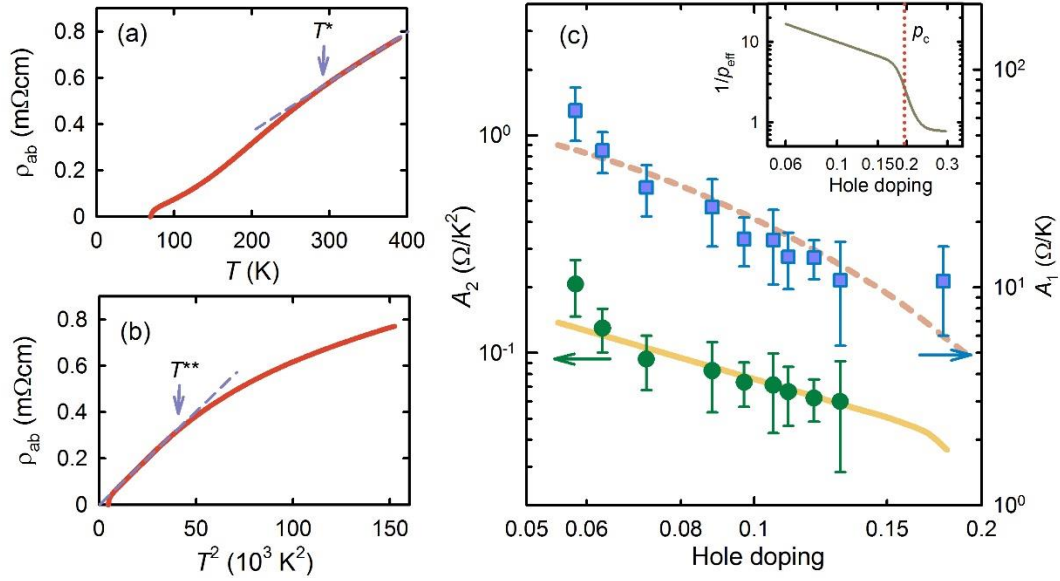


Figure 3 | Resistivity coefficients of Hg1201. Resistivity of the UD71 sample on an (a) linear and (b) quadratic temperature scale, with characteristic temperatures T^* and T^{**} and the linear and quadratic slopes (coefficients) A_1 and A_2 . (c) Linear (circles) and quadratic (squares) resistivity coefficients of Hg1201, obtained by fitting the data above T^* and below T^{**} , respectively, as in (a) and (b). The lines are obtained from the model, with the same parameters as in Fig. 1c. The quadratic coefficient is consistent with $A_2 \sim 1/p$ up to about optimal doping. Note that in the model $A_2 \sim 1/p_{\text{eff}}(p,0)$, since the low-temperature asymptotic behavior is always quadratic in temperature. The model yields A_1 without free parameters once A_2 is given, and thus correctly predicts the absolute value of the ratio A_1/A_2 . The inset gives $1/p_{\text{eff}}(p,0)$ from Eq. (1) in a wide doping range and demonstrates the smooth drop around p_c .

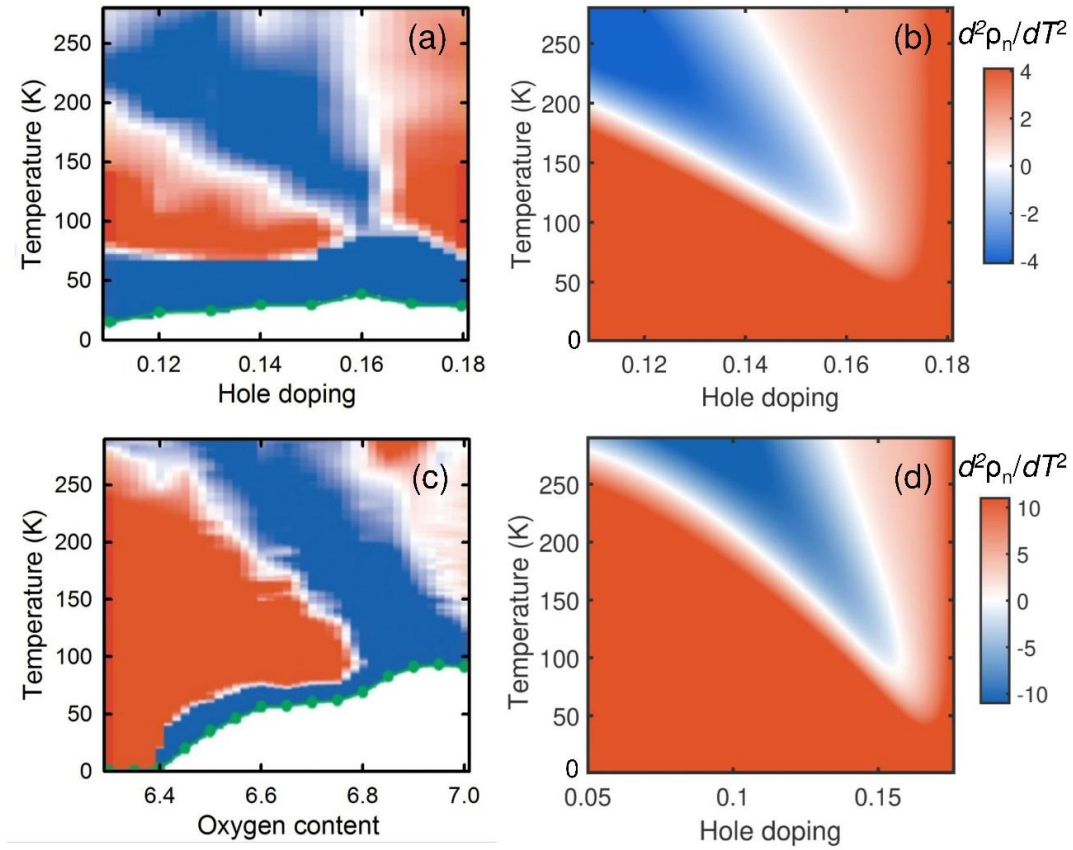


Figure 4 | Resistivity phase diagrams of other cuprate families. (a) Experimental and (b) model resistivity phase diagram for BSLCO, and (c) experimental and (d) model phase diagram for YBCO. The data are from ref. [3], and the model parameters are listed in Table 1. Experimental resistivity curves are normalized to the values at 280 K (BSLCO) and 290 K (YBCO); calculated curvatures are normalized by $p_{\text{eff}}(p,0)$.

	Δ_0	δ	p_c	α
Hg1201	3800 K	700 K	0.197	2
LSCO	3900 K	800 K	0.22	2
BSLCO	4300 K	700 K	0.175	4
YBCO	4500 K	500 K	0.177	2

Table 1. Gap distribution parameters for four cuprate families. The parameters for LSCO are from ref. [22].

References

- ¹ Keimer, B., Kivelson, S. A., Norman, M. R., Uchida, S. & Zaanen, J. From quantum matter to high-temperature superconductivity in copper oxides. *Nature* **518**, 179-186 (2015)
- ² Takagi, H. *et al.* Systematic evolution of temperature-dependent resistivity in $\text{La}_{2-x}\text{Sr}_x\text{CuO}_4$. *Phys. Rev. Lett.* **69**, 2975 (1992)
- ³ Ando, Y., Komiyama, S., Segawa, K., Ono, S. & Kurita, Y. Electronic phase diagram of high- T_c cuprate superconductors from a mapping of the in-plane resistivity curvature. *Phys. Rev. Lett.* **93**, 267001 (2004)
- ⁴ Cooper, R. A. *et al.*, Anomalous criticality in the electrical resistivity of $\text{La}_{2-x}\text{Sr}_x\text{CuO}_4$. *Science* **323**, 603-607 (2009)
- ⁵ N. Barišić *et al.*, Universal sheet resistance and revised phase diagram of the cuprate high-temperature superconductors. *Proc. Nat. Acad. Sci. USA* **110**, 12235-12240 (2013)
- ⁶ Hussey, N. E., Abdel-Jawad, M., Carrington, A., Mackenzie, A. P. & Balicas, L. A coherent three-dimensional Fermi surface in a high-transition-temperature superconductor. *Nature* **425**, 814-817 (2003)
- ⁷ Plate, M. *et al.*, Fermi surface and quasiparticle excitations of overdoped $\text{Tl}_2\text{Ba}_2\text{CuO}_{6+\delta}$. *Phys. Rev. Lett.* **95**, 077001 (2005)
- ⁸ Pasupathy, A. N. *et al.*, Electronic origin of the inhomogeneous pairing interaction in the high- T_c superconductor $\text{Bi}_2\text{Sr}_2\text{CaCu}_2\text{O}_{8+\delta}$. *Science* **320**, 196-201 (2008)
- ⁹ Chan, M.-K. *et al.*, In-plane magnetoresistance obeys Kohler's rule in the pseudogap phase of cuprate superconductors. *Phys. Rev. Lett.* **113**, 177005 (2014).
- ¹⁰ Mirzaei, S-I. *et al.* Spectroscopic evidence for Fermi-liquid-like energy and temperature dependence of the relaxation rate in the pseudogap phase of the cuprates. *Proc. Nat. Acad. Sci. USA* **110**, 5774-5778 (2013).
- ¹¹ Barišić, N. *et al.* Hidden Fermi liquid behavior throughout the phase diagram of the cuprates. *arxiv:1507.07885* (2015).
- ¹² Li, Y., Tabis, W., Yu, G., Barišić, N. & Greven, M. Hidden Fermi-liquid charge transport in the antiferromagnetic phase of the electron-doped cuprate superconductors. *Phys. Rev. Lett.* **117**, 197001 (2016).
- ¹³ Vishik, I. M. Photoemission perspective on pseudogap, superconducting fluctuations, and charge order in cuprates: a review of recent progress. *Rep. Prog. Phys.* **81**, 062501 (2018)
- ¹⁴ Rybicki, D. *et al.* Two-component uniform spin susceptibility of superconducting $\text{HgBa}_2\text{CuO}_{4+\delta}$ single crystals measured using ^{63}Cu and ^{199}Hg nuclear magnetic resonance. *Phys. Rev. B* **85**, 104517 (2012).
- ¹⁵ Storey, J. G. & Tallon, J. L. Two-component electron fluid in underdoped high- T_c cuprate superconductors. *Europhys. Lett.* **98**, 17011 (2012).
- ¹⁶ Alldredge, J. W., Fujita, K., Eisaki, H., Uchida, S. & McElroy, K. Universal disorder in $\text{Bi}_2\text{Sr}_2\text{CaCu}_2\text{O}_{8+x}$. *Phys. Rev. B* **87**, 104520 (2013)

- ¹⁷ Singer, P. W., Hunt, A. W. & Imai, T. , ⁶³Cu NQR evidence for spatial variation of hole concentration in $\text{La}_{2-x}\text{Sr}_x\text{CuO}_4$. *Phys. Rev. Lett.* **88**, 047602 (2002)
- ¹⁸ Bobroff, J. *et al.*, Absence of static phase separation in the high- T_c cuprate $\text{YBa}_2\text{Cu}_3\text{O}_{6+y}$. *Phys. Rev. Lett.* **89**, 157002 (2002)
- ¹⁹ Rybicki, D. *et al.* Spatial inhomogeneities in single-crystal $\text{HgBa}_2\text{CuO}_{4+\delta}$ from ⁶³Cu NMR spin and quadrupole shifts. *J Supercond. Nov. Magn.* **22**, 179 (2008)
- ²⁰ Campi, G. *et al.* Inhomogeneity of charge-density-wave order and quenched disorder in a high- T_c superconductor. *Nature* **525**, 359 (2015)
- ²¹ Mesot, J. *et al.* Neutron spectroscopic evidence for cluster formation and percolative superconductivity in $\text{ErBa}_2\text{Cu}_3\text{O}_x$. *Phys. Rev. Lett.* **70**, 865 (1993)
- ²² Pelc, D., Popčević, P., Požek, M., Greven, M. & Barišić, N. Unusual behavior of cuprates explained by heterogeneous charge localization. *Sci. Adv.* **5**, eaau4538 (2019)
- ²³ Barišić, N. *et al.* Demonstrating the model nature of the high-temperature superconductor $\text{HgBa}_2\text{CuO}_{4+\delta}$. *Phys. Rev. B* **78**, 054518 (2009)
- ²⁴ Barišić, N. *et al.* Universal quantum oscillations in the underdoped cuprate superconductors. *Nat. Phys.* **9**, 761 (2013)
- ²⁵ Li, Y., Egetenmeyer, N., Gavilano, J. L., Barišić, N. & Greven, M. Magnetic vortex lattice in $\text{HgBa}_2\text{CuO}_{4+\delta}$ observed by small-angle neutron scattering. *Phys. Rev. B* **83**, 054507 (2011)
- ²⁶ Vishik, I. M. *et al.* Angle-resolved photoemission spectroscopy study of $\text{HgBa}_2\text{CuO}_{4+\delta}$. *Phys. Rev. B* **89**, 195141 (2014)
- ²⁷ Ino, A. *et al.* Doping-dependent evolution of the electronic structure of $\text{La}_{2-x}\text{Sr}_x\text{CuO}_4$ in the superconducting and metallic phases. *Phys. Rev. B* **65**, 094504 (2002)
- ²⁸ Fournier, D. *et al.*, Loss of nodal quasiparticle integrity in underdoped $\text{YBa}_2\text{Cu}_3\text{O}_{6+x}$. *Nat. Phys.* **6**, 905 (2010)
- ²⁹ W. J. Padilla *et al.*, Constant effective mass across the phase diagram of high- T_c cuprates. *Phys. Rev. B* **72**, 060511(R) (2005)
- ³⁰ Ono, S., Komiyama, S. & Ando, Y. Strong charge fluctuations manifested in the high-temperature Hall coefficient of high- T_c cuprates. *Phys. Rev. B* **75**, 024515 (2007)
- ³¹ Drozdov, I. K. *et al.* Phase diagram of $\text{Bi}_2\text{Sr}_2\text{CaCu}_2\text{O}_{8+\delta}$ revisited. *Nat. Commun.* **9**, 5210 (2018)
- ³² Legros, A. *et al.* Universal T -linear resistivity and Planckian limit in overdoped cuprates. *arxiv:1805.02512* (2018)
- ³³ Gegenwart, P., Si, Q. & Steglich, F. Quantum criticality in heavy-fermion metals. *Nat. Phys.* **4**, 186-197 (2008)
- ³⁴ Daou, R. *et al.* Linear temperature dependence of resistivity and change in the Fermi surface at the pseudogap critical point of a high- T_c superconductor. *Nat. Phys.* **5**, 31 (2009)
- ³⁵ Taillefer, L. Scattering and pairing in cuprate superconductors. *Annu. Rev. Cond. Matter Phys.* **1**, 51 (2010)

- ³⁶ Gor'kov, L. P. & Teitel'baum, G. B. Interplay of externally doped and thermally activated holes in $\text{La}_{2-x}\text{Sr}_x\text{CuO}_4$ and their impact on the pseudogap crossover. *Phys. Rev. Lett.* **97**, 247003 (2006)
- ³⁷ Luo, N. & Miley, G. H. Kohler's rule and relaxation rates in high- T_c superconductors. *Physica C* **371**, 259 (2002)
- ³⁸ Ando, Y., Kurita, Y., Komiya, S., Ono, S. & Segawa, K. Evolution of the Hall coefficient and the peculiar electronic structure of the cuprate superconductors. *Phys. Rev. Lett.* **92**, 197001 (2004)
- ³⁹ Badoux, S. *et al.* Change of carrier density at the pseudogap critical point of a cuprate superconductor. *Nature* **531**, 210 (2016)
- ⁴⁰ Grissonnanche, G. *et al.*, Direct measurement of the upper critical field in cuprate superconductors. *Nat. Commun.* **5**, 3280 (2014)
- ⁴¹ Büchner, B., Breuer, M., Freimuth, A. & Kampf, A. P. Critical buckling for the disappearance of superconductivity in rare-earth-doped $\text{La}_{2-x}\text{Sr}_x\text{CuO}_4$. *Phys. Rev. Lett.* **73**, 1841 (1994)
- ⁴² Wakimoto, S. *et al.* Incommensurate lattice distortion in the high temperature tetragonal phase of $\text{La}_{2-x}(\text{Sr},\text{Ba})_x\text{CuO}_4$. *J. Phys. Soc. Jpn.* **75**, 074714 (2006)
- ⁴³ Markiewicz, R. S. A survey of the van Hove scenario for high- T_c superconductivity with special emphasis on pseudogaps and striped phases. *J. Phys. Chem. Solids* **58**, 1179-1310 (1997)
- ⁴⁴ Eisaki, H. *et al.*, Effect of chemical inhomogeneity in bismuth-based copper oxide superconductors. *Phys. Rev. B* **69**, 064512 (2004)
- ⁴⁵ Rullier-Albenque, F., Alloul, H. & Tourbot, R. Disorder and transport in cuprates: weak localization and magnetic contributions. *Phys. Rev. Lett.* **87**, 157001 (2001)
- ⁴⁶ Gunnarson, O, Calandra, M. & Han, J. E. Saturation of electrical resistivity. *Rev. Mod. Phys.* **75**, 1085 (2003).
- ⁴⁷ Ghiringhelli, G. *et al.* Long-range incommensurate charge fluctuations in $(\text{Y},\text{Nd})\text{Ba}_2\text{Cu}_3\text{O}_{6+x}$. *Science* **337**, 821 (2012)
- ⁴⁸ Hücker, M. *et al.* Competing charge, spin, and superconducting orders in underdoped $\text{YBa}_2\text{Cu}_3\text{O}_y$. *Phys. Rev. B* **90**, 054514 (2014)
- ⁴⁹ Tabis, W. *et al.*, Charge order and its connection with Fermi-liquid charge transport in a pristine high- T_c cuprate. *Nat. Commun.* **5**, 5875 (2014)
- ⁵⁰ Tabis, W. *et al.* Synchrotron x-ray scattering study of charge-density-wave order in $\text{HgBa}_2\text{CuO}_{4+\delta}$. *Phys. Rev. B* **96**, 134510 (2017)
- ⁵¹ Hinton, J. P. *et al.* The rate of quasiparticle recombination probes the onset of coherence in cuprate superconductors. *Sci. Rep.* **6**, 23610 (2016)
- ⁵² Arpaia, R. *et al.* Dynamical charge density fluctuations pervading the phase diagram of a Cu-based high- T_c superconductor. *arxiv:180904949* (2018)
- ⁵³ Laliberte, F. *et al.* Fermi-surface reconstruction by stripe order in cuprate superconductors. *Nat. Commun.* **2**, 432 (2011)

- ⁵⁴ Chan, M. K. et al., Single reconstructed Fermi surface pocket in an underdoped single-layer cuprate superconductor. *Nat. Commun.* **7**, 12244 (2016)
- ⁵⁵ Honma, T. & Hor, P. H. Unified electronic phase diagram for hole-doped high- T_c cuprates. *Phys. Rev. B* **77**, 184520 (2008) and references therein
- ⁵⁶ Uchida, S. et al. Optical spectra of $\text{La}_{2-x}\text{Sr}_x\text{CuO}_4$: effect of carrier doping on the electronic structure of the CuO_2 plane. *Phys. Rev. B* **43**, 7942 (1992)
- ⁵⁷ Lee, Y. S. et al. Electrodynamics of the nodal metal state in weakly doped high- T_c cuprates. *Phys. Rev. B* **72**, 054529 (2005)
- ⁵⁸ Ahn, K. H., Lookman, T. & Bishop, A. R., Strain-induced metal-insulator phase coexistence in perovskite manganites. *Nature* **428**, 401 (2004)
- ⁵⁹ Phillips, J. C., A. Saxena, A. & Bishop, A. R. Pseudogaps, dopands, and strong disorder in cuprate high-temperature superconductors. *Rep. Prog. Phys.* **66**, 2111-2182 (2003).
- ⁶⁰ Krumhansl, J. A. Fine scale mesostructures in superconducting and other materials, in Lattice Effects in High- T_c Superconductors: Proceedings of the Conference, Santa Fe, New Mexico, January 13-15, 1992
- ⁶¹ Keimer, B. et al. Magnetic excitations in pure, lightly doped, and weakly metallic La_2CuO_4 . *Phys. Rev. B* **46**, 14034 (1992)
- ⁶² Zhao, L. et al. A global inversion-symmetry-broken phase inside the pseudogap region of $\text{YBa}_2\text{Cu}_3\text{O}_y$. *Nat. Phys.* **13**, 250 (2017)
- ⁶³ Zhao, X. et al. Crystal growth and characterization of the model high-temperature superconductor $\text{HgBa}_2\text{CuO}_{4+\delta}$. *Adv. Mater.* **18**, 3243 (2006)
- ⁶⁴ Yamamoto, A., Hu, W.-Z. & Tajima, S. Thermoelectric power and resistivity of $\text{HgBa}_2\text{CuO}_{4+\delta}$ over a wide doping range. *Phys. Rev. B* **63**, 024504 (2000)
- ⁶⁵ Nakamae, S. et al. Electronic ground state of heavily overdoped nonsuperconducting $\text{La}_{2-x}\text{Sr}_x\text{CuO}_4$. *Phys. Rev. B* **68**, 100502(R) (2003).
- ⁶⁶ Proust, C., Vignolle, B., Levallois, J., Adachi, S. & Hussey, N. E. Fermi liquid behavior of the in-plane resistivity in the pseudogap state of $\text{YBa}_2\text{Cu}_4\text{O}_8$. *Proc. Nat. Acad. Sci. USA* **113**, 13654-13659 (2016).